ICAS 2016
30th Congress of the International Council of the Aeronautical Sciences
DCC, Daejeon, Korea ; September 25-30, 2016

NON-INTRUSIVE UNSTEADY PSP TECHNIQUE FOR INVESTIGAYION OF TRANSONIC BUFFETING

Yosuke SUGIOKA*, Kazuyuki NAKAKITA, and Keisuke ASAI***
***Tohoku University, Sendai, Japan, **Japan Aerospace Exploration Agency, Tokyo, Japan**

Keywords: *Transonic Buffet, Pressure-Sensitive Paint, Unsteady Measurement*

Abstract

In this study, transonic buffeting phenomena on a 2D airfoil and a 3D transport wing were analyzed with unsteady pressure-sensitive paint measurement. Polymer/ceramic PSPs with low surface roughness were applied to 2D- and 3D-Common Research Models in order to measure unsteady pressure distributions without intruding the flows. Unsteady pressure fields on the 2D airfoil were evaluated at Mach number of 0.74 and chord Reynolds number of 5 × 10^6. Pressure waves moving upstream at the angle of attack of 3° and a periodic shock oscillation under buffeting condition were clearly measured. A spectral analysis showed that the fundamental reduced frequency of the shock oscillation was 0.42 at the angle of attack of 6°. To demonstrate the effectiveness of unsteady PSP measurement on a 3D transport wing, wind-tunnel testing was conducted at Mach number of 0.85 and chord Reynolds number of 1.54 × 10^6. Pressure time histories and their spectra measured by the PSP agreed well with those obtained by an unsteady pressure transducers. Under the off-design conditions, complicated shock oscillations on the swept wing were observed. These results indicate that the PSPs can offer a powerful means to investigate transonic buffeting on aircraft.

1 Introduction

Upper limits of cruising flight of transport aircraft are limited by transonic buffeting characterized by large-scale lift oscillations. Therefore, it is necessary to clarify the mechanisms of buffeting and predict the buffet onset.

Transonic buffeting has been an object of study for more than 60 years. Thus many experiments and computer simulations have been conducted in order to analyze transonic buffeting on both two-dimensional airfoils [1] and three-dimensional wings [2-4].

However, the mechanisms of buffeting are not yet fully understood. Particularly, unsteady flow on a 3D wing is too complicated to be analyzed by using low-resolution pressure information acquired with conventional pressure transducers. Therefore, a new method to provide pressure distributions with high spatiotemporal resolutions is indispensable.

In recent years, unsteady pressure-sensitive paint (PSP) has attracted much attention from the aerospace community, as a means to measure pressure distributions with high spatiotemporal resolutions. Polymer/ceramic PSP (PC-PSP) composed of polymer and ceramic particles (Fig. 1) is one of the most common unsteady PSPs.

The time response of PSP is governed by the diffusion process of oxygen through the coating. Usually, a large amount of particles are added to PC-PSP in order to increase gas diffusivity of the binder. However, these particles make the painted model surface rougher than a clean one.

The surface roughness of PSP coating has an adverse effect on transonic flow. As an example, Sugioka et al. found noticeable effects of surface roughness on the balance measurement in a transonic wind-tunnel test of a generic transport model painted with PC-PSP [5].

In order to realize non-intrusive unsteady PSP measurement, we need to find a way to

satisfy two contradictory requirements for PC-PSP coating: high gas diffusivity and low surface roughness. To solve this problem, systematic tests were conducted for PC-PSP samples having different formulations. As a result, PC-PSPs with low surface roughness (designated MOD-2 and MOD-3) have been developed and their effectiveness for unsteady measurement in a transonic flow was verified by experiment [6].

In this study, the unsteady PSPs with low surface roughness are applied to measure unsteady pressure fields caused by transonic buffeting on a 2D airfoil and a 3D transport wing. The effects of surface roughness of the PSPs are evaluated in each wind-tunnel test. For the 2D airfoil, time-series pressure fields and RMS pressure fluctuations are obtained. Then, the dominant frequencies are clarified with a spectral analysis. For the 3D transport wing, unsteady PSP data are validated using a pressure transducer. Then transonic buffeting phenomena on the 3D transport wing are analyzed based on the time-averaged and time-series pressure distributions and RMS pressure fluctuations.

2 Unsteady PSP with Low Surface Roughness

A fully turbulent boundary layer should not be affected by a surface roughness unless the roughness elements project out of purely viscous sublayer δ_υ [7]. In other words, a surface can be regarded as a smooth wall if the roughness height k^+ (= k/δ_υ) is smaller than the admissible roughness k^+_{adm} = 5. Therefore, PSP coating having surface roughness smaller than this admissible roughness has to be used to realize non-intrusive measurement.

Sugioka et al. have developed unsteady PSPs satisfying the requirement of admissible roughness [6]. In this study, MOD-2 and MOD-3 were selected and applied to a 3D transport wing and a 2D airfoil, respectively.

Table 1 presents arithmetic average roughness and technical roughness of the PSP coatings applied to wind-tunnel models. We have confirmed that both PSPs satisfy the requirement of admissible roughness under the test conditions in this study. Figures 2a and 2b show pressure sensitivities and bode plots of these PSPs. From Fig. 2b, it is found that the cutoff frequencies (Gain = -3 dB) are higher than 2 kHz.

3 Description of Experiments

3.1 2D Airfoil

The wind tunnel test of a 2D airfoil was conducted in the JAXA 0.8 x 0.45 m High-Reynolds Number Transonic Wind Tunnel (JTWT2) at the JAXA Chofu Aerospace Center. The JTWT2 is a blow-down type wind tunnel that has a test section of 0.8 m (height) by 0.45 m (width) in cross section and 2.45 m in length. Boundary layers on the upstream side walls are sucked through rigimesh plates in order to reduce effects of the side walls.

In this study, a reference airfoil of the NASA Common Research Model (2D-CRM) [8, 9] was used as a test article. The airfoil was based on the cross section of the CRM wing at the spanwise location, η = 0.65. The model has 80 pressure taps on the surface. The 2D-CRM installed in the JTWT2 is shown in Fig. 3. The chord and the span length are 0.2 m and 0.45 m, respectively. Trip disks (Aeronautical trip dots, 3.1 mil silver matte, CAD Cut Inc.) were applied at 10% chord of the model in order to fix boundary-layer transition location.

The free-stream Mach number was set at 0.74 and the Reynolds number calculated based on the chord length was 5.0 x 10^6. Angles of attack and pressure coefficients for the 2D airfoil presented in this paper are values uncorrected for the wall inference effects.

Figure 4 shows a schematic illustration of the PSP measurement system in the JTWT2. Two UV-LEDs (IL-106, Hardsoft) and a high-speed camera (Phantom v1211, Vision research) were used as a detector of PSP luminescence and illumination light sources, respectively. A band-pass optical filter (590-710 nm) was mounted in front of the camera lens. The frame rate of the high-speed camera was set at 5000 fps.

Pressure distribution on the model was measured by pressure taps and scanning type pressure gauges. The pressure measurement

with sampling time of 1 ms was repeated 20 times, and the acquired data were averaged for each pressure tap. In this paper, the results averaged for 3 runs are shown.

3.2 3D Transport Wing

The JAXA 2 m Transonic Wind Tunnel (JTWT1) was used for the experiment of a 3D transport wing. The JTWT1 is a closed-circuit and continuous-flow wind tunnel that has a test section with 2 m x 2 m square in cross section and 4.13 m in length.

An 80%-scale model of the NASA Common Research Model (3D-CRM) [10, 11] was used as a test article. Figure 5 shows the 3D-CRM installed in the JTWT1. The mean aerodynamic chord c_{mac} of the model is 0.1513 m. This model has 325 pressure taps and 4 Kulite sensors on the main wings. In this study, the Kulite sensor located at x/c = 0.689 and η = 0.731 was used to validate the acquired PSP data. Here, x and c are model streamwise location and chord length, respectively. A 6-component internal balance was installed inside the model fuselage and attached to a blade support sting in order to measure the aerodynamic forces and moments acting on the model. Similarly to the 2D-CRM, trip disks (Aeronautical trip dots, silver matte, CAD Cut Inc.) were applied on the wings and the fuselage. The heights of the trip disks are shown in Table 2.

The free stream Mach number and the total pressure were set at 0.85 and 80 kPa, respectively. The Reynolds number calculated based on c_{mac} was 1.54 x 10^6. It is noted that the Reynolds number in this test was lower than the JAXA's standard test condition of the 3D-CRM (Re_C = 2.27 x 10^6).

The MOD-2 polymer/ceramic binder was selected for the 3D-CRM. It is easily polished and it has higher pressure-sensitivity than the MOD-3. Although surface roughness of the MOD-2 is larger than that of the MOD-3, it still satisfies the criteria for admissible roughness under the test condition of the 3D-CRM. The wings and the horizontal stabilizers of the model were painted with the binder. Then, PtTFPP was sprayed and adsorbed on the pre-coated binder surface on the right wings.

The PSP measurement system in the JTWT1 is shown in Fig. 6. The high-speed camera and the LEDs were the same devices used in the experiment of the 2D airfoil. The frame rate of the camera was set at 2000 fps or 7000 fps.

Surface static pressure distribution was measured by pressure taps and ESP pressure scanners housed inside the model fuselage. Simultaneously with the PSP measurement, dynamic pressure measurement was conducted using Kulite sensors, a DC amplifier, and a data logger. The sampling rate of the data logger was set at 50 kHz. In this experiment, angles of attack were corrected based on the standard procedure for the JTWT1.

3.3 Data Processing

In order to calculate pressure coefficients on the models, wind-on and wind-off PSP images were obtained. The wind-on images were acquired during runs, and the wind-off images were acquired at the atmospheric pressure around 100 kPa. A dark image was subtracted from all images. A time-averaged wind-on image I_{ave} and a reference image I_{ref} were prepared by averaging the wind-on images and the wind-off images. In this study, the *in-situ* calibration method was used to convert the measured PSP data to pressures. Coefficients A, B, and C in the calibration equation (1) were determined by fitting PSP intensity ratio I_{ref}/I_{ave} near pressure taps and pressure coefficients measured with the pressure taps to Eq. (2). For the 2D airfoil test, the data measured by pressure taps placed on the model 1/2 span (center line) were used for calibration. For the 3D transport wing test, pressure coefficients acquired by pressure taps located at η = 0.3971 were used for calibration. Pressure distributions on the models were calculated in accordance with the calibration equation (1).

$$C_P = A \cdot \left(\frac{I_{ref}}{I} \right)^2 + B \cdot \left(\frac{I_{ref}}{I} \right) + C \qquad (1)$$

$$C_{P,pressuretap} = A \cdot \left(\frac{I_{ref}}{I_{ave}} \right)^2 + B \cdot \left(\frac{I_{ref}}{I_{ave}} \right) + C \qquad (2)$$

The root-mean-square (RMS) pressure fluctuations were calculated from time-series pressure images. For the 2D airfoil, fast Fourier transform (FFT) analysis was performed on the pressure variations to find characteristic frequencies and, for the 3D transport wing, to compare the PSP data with the spectra measured by the Kulite sensor. The frequency resolutions of the PSP data Δf was 1.22 Hz for the 2D airfoil and 1.71 Hz for the 3D transport wing.

4 Results and Discussions

4.1 2D Airfoil

4.1.1 Comparison of Pressure Distribution between Paint-on and Paint-off Conditions

Figure 7 shows a comparison of time-averaged pressure distributions between paint-off and paint-on conditions.

This figure indicates that the pressure distributions are almost the same for paint-on and paint-off conditions, meaning that MOD-3 binder does not affect the flow on the 2D airfoil.

At α = 3.0°, there can be seen a pressure increase at x/c = 0.3 and an area having small pressure gradient around x/c = 0.35-0.5. This is a pressure profile corresponding to a lambda shock structure. At α = 5.0°, pressure increases rapidly at x/c = 0.5 by a strong normal shock wave on the airfoil. At α = 6.0°, the pressure gradient on the upper surface of the airfoil become smoother. This indicates that the shock wave oscillates in the chordwise direction and the buffeting occurs.

4.1.2 Unsteady Pressure Distributions

Figures 8a, 8b and 8c show the x-t diagrams of time-series pressure on the airfoil at α = 3.0°, 5.0°, and 6.0°, respectively. Three pixel lines on the span center line captured from the time-series pressure images are lined up along the time axis. Figure 9 shows the RMS distributions on the model.

Characteristic unsteady pressure fields and RMS distributions are changed with the angle of attack. Therefore, unsteady flow on the airfoil is discussed for each angle of attack.

As shown in Fig. 8a, propagation of pressure waves and a movement of a foot of the lambda shock wave can be seen at α = 3.0°. Figure 9a shows that there are two distinct areas having large RMS; the first one is a narrow line at x/c = 0.3 that corresponds to an oscillation of the shock wave, and the second one is a wide area distributed on the mid-chord of the airfoil that corresponds to a propagation of pressure waves.

In Fig. 8b (α = 5.0°), a sharp pressure increase is present at x/c = 0.5 and its position slightly oscillates. Contrary to α = 3.0°, pressure waves moving upstream are not seen clearly at this angle of attack. A distinct high-low pressure line observed downstream of the shock wave is a shadow caused by excitation light refracted by the normal shock wave. From Fig. 9b, it is found that there are two narrow lines with larger RMS caused by an oscillation of the shock wave and its projected image.

Figure 8c shows that, at α = 6.0°, a shock wave periodically oscillates on the airfoil, indicating that buffeting occurs. The movement track of the shock wave is almost sinusoidal. It is seen in Fig. 8c that pressure downstream of the shock wave also fluctuates periodically. When the shock wave moves upstream, pressure decreases downstream of the shock wave. This phenomenon can be caused by a separation of the boundary layer and corresponding upstream movement of the shock wave. As shown in Fig. 9c, RMS pressure fluctuations increase at α = 6.0°. The region with $(C_P)_{RMS}$ = 0.25-0.35 is regarded as an area where an oscillating shock wave exists. It is noted that three-dimensionality of RMS distribution appears in this case.

4.1.4 Dominant Frequencies of Pressure Fluctuations

Figures 10a, 10b, and 10c present power spectral density (PSD) of pressure fluctuations at α = 3.0°, 5.0°, and 6.0°, respectively. Horizontal axes show reduced frequency $\kappa = 2\pi f/U$, where U [m/s] is the free stream velocity.

Figure 10a shows PSD at the position of the front shock of the lambda shock structure. It is

clear that there are two peak frequencies: 3.06 (587 Hz) and 6.13 (1176 Hz). These frequencies correspond to upstream propagations of the pressure waves. Broadband components are prominent at κ less than 0.7 (134 Hz) too, suggesting that the shock wave oscillates in this wide frequency range.

Figure 10b presents PSD at the foot of the normal shock wave. Characteristic frequencies at κ = 3.07 and 6.13 are observed in the spectrum, meaning that pressure waves moving upstream also appear at α = 5.0°. Their amplitude are smaller than those at α = 3.0°. In addition to these peak frequencies, broadband low-frequency components of the shock oscillation are also observed.

Figure 10c provides PSD at the chordwise station with the peak RMS, which is regarded as the center of the shock oscillation. In Fig. 10c, a pressure fluctuation at κ = 0.42 (80.6 Hz) and its harmonic components become larger. The shock wave on the airfoil can be considered to oscillate at this fundamental frequency.

4.2 3D Transport Wing

4.2.1 Comparison of Aerodynamic Forces between Paint-on and Paint-off Conditions

Figures 11a and 11b show lift coefficient and drag coefficient of the 3D-CRM, respectively. In these figures, the data measured under paint-off and paint-on conditions are represented by red diamonds and blue squares. Also, the differences between the two data, which are calculated using spline interpolation, are shown as a green line.

From Fig. 11a and 11b, it is found that there are no significant differences in lift or drag between the paint-off and paint-on conditions below α = 4°. At α = 4° or higher, however, both lift and drag for the paint-on run are larger than those for the paint-off run. These changes differ from the results reported in previous studies [6, 12]. It is likely that a change in aerodynamic forces is caused by the mechanisms different from the roughness effect. One possible cause is a slight change in the spanwise positions of trip disks due to reapplication. For the reasons mentioned above, it can be concluded that the effect of the PSP coating itself on the flow is negligibly small.

4.2.2 Validation of Unsteady PSP data by Pressure Transducer

Figure 12 and 13 shows pressure time-histories and its spectra measured either by the Kulite sensor and the PSP. The Kulite data are presented as the time average value of seven data points corresponding to the camera exposure time (140 μs) and the sampling time of the data logger (20 μs).

Figure 12 indicates that the pressure variation is only 2.5 kPa or smaller at the Kulite position. Nevertheless, the PSP data agree well with those acquired by the Kulite sensor. In addition, PSD of ΔC_P measured by the Kulite sensor and that by the PSP are almost the same, including a bump around 800 Hz at α = 4.72°.

4.2.3 Time-Averaged Pressure and RMS Pressure Fluctuations Distributions

Figures 14a to 14c show time-averaged pressure distributions acquired by the PSP at α = 2.85° (cruise condition), 4.72° and 6.58° (off-design conditions), respectively. RMS distributions on the wing are also presented in Fig. 15.

The details of time-averaged pressure distributions are clearly visualized in Fig. 14 and the areas with large pressure fluctuations in Fig. 15, under both cruise and off-design conditions.

Figures 14a and 15a indicate that pressure on the wing is stable under the cruise condition (α = 2.85°). However, there is a small pressure fluctuation at the outboard of the wing. This is considered to be caused by the unsteadiness of a lambda shock structure.

At α = 4.72°, pressure near the trailing edge around mid-span decreases, meaning that the boundary layer separation occurs in this area. Under this condition, the shock wave begins to oscillate at outboard of the wing and RMS pressure fluctuations become large around the trading edge. This indicates that unsteady separation of boundary layers happens.

At α = 6.58°, the time-averaged position of the shock wave moves upstream and a large-amplitude shock oscillation occurs. Figure 15c shows that the movement of the shock wave

varies depending on the spanwise station. Also noted are small structures of RMS distribution seen at around the kink. They might be caused by interactions between the shock wave and vortices.

4.2.4 Time-Series Pressure Distributions under Buffeting Condition

Time-series pressure distributions and the corresponding dynamic components at α = 6.58° are shown in Figs. 16a and 16b, respectively. In Fig. 16b, the red area means that pressure is higher than the average; the blue area means that the opposite is the case.

From these figures, it is found that the shock oscillation on the wing is considerably complicated and three-dimensional. The area in which pressure is higher than the average moves toward the outboard of the wing. This suggests that the oscillation of the shock wave on the swept wing contains two components: one is moving in the chordwise direction and the other is in the spanwise direction.

4 Concluding Remarks

To investigate transonic buffeting on the 2D airfoil and the 3D transport wing, unsteady PSP measurement was conducted. PC-PSPs with low surface roughness were used in these experiments.

The PC-PSPs did not affect the flow on both the 2D airfoil and the 3D transport wing. Therefore, it can be concluded that the paint surface is smooth enough to realize non-intrusive PSP measurement in transonic flow.

In the experiment of the 2D airfoil, unsteady PSP could capture pressure waves moving upstream at lower angle of attack and a periodic shock oscillation under the buffeting condition. Also, the dominant frequencies of the phenomena were identified using the spectral analysis.

In the experiment of the 3D transport wing, unsteady PSP could visualize complicated shock movements under the buffeting condition. A shock oscillation on the swept wing contains two phenomena that propagate in the chordwise direction and the spanwise directions.

These wind tunnel tests have demonstrated the effectiveness of unsteady PSP measurement to investigate transonic buffet phenomena. By applying the correlation analysis and the fast-Fourier transform, passage of pressure-wave propagation and the frequency of shock oscillation can be identified clearly. The PSP measurement also can provide the verification data for computational fluid dynamics.

References

[1] Lee BHK. Self-sustained shock oscillations on airfoils at transonic speeds. *Progress in Aerospace Sciences*, Vol. 37, pp. 147-196, 2001.

[2] Roos FW. The Buffeting Pressure Field of a High-Aspect-Ratio Swept Wing. *18th AIAA Fluid Dynamics and Plasmadynamics and Lasers Conference*, Cincinatti, Ohio, AIAA-85-1609, July 16-18, 1985.

[3] Molton P, Dandois J, Lepage A, Brunet V and Bur A. Control of buffet phenomenon on a transonic swept wing. *AIAA J*., 51(4), pp. 761–772, 2013.

[4] Dandois J. Experimental study of transonic buffet phenomenon on a 3D swept wing. P*hysics of Fluids*, 28, 016101, 2016.

[5] Sugioka Y, Numata D, Asai K, Nakakita K, Koike S and Koga S. Unsteady PSP Measurement of Transonic Buffet on a Wing. *53rd AIAA Aerospace Sciences Meeting*, Kissimmee, Florida, AIAA2015-0025, 5-9 January, 2015.

[6] Sugioka Y, Numata D, Asai K, Koike S, Nakakita K and Nakajima T. Polymer/Ceramic PSP with Reduced Surface Roughness for Unsteady Pressure Measurement in Transonic Flow. *54rd AIAA Aerospace Sciences Meeting*, San Diego, California, AIAA2016-2018, 4-8 January, 2016.

[7] Schlichting H. *Boundary-Layer Theory 8th Edition*, McGraw-Hill, New York, 1999.

[8] CRM.65 airfoil sections, http://commnonresearchmodel.larc.nasa.gov/crm-65-airfoil-sections/ [cited 24 June 2014].

[9] Koike S, Nakakita K, Nakajima T, Koga S, Sato M, Kanda H, Kusunose K, Murayama M, Ito Y, Yamamto K. Experimental Investigation of Vortex Generator Effect on Two- and Three- Dimensional NASA Common Research Models. *53rd AIAA Aerospace Sciences Meeting*, Kissimmee, Florida, AIAA2015-0025, 5-9 January, 2015.

[10] Vassberg JC, DeHaan MA, Rivers MS and Wahls RA. Development of a Common Research Model for Applied CFD Validation Studies. *26th AIAA Applied Aerodynamics Conference*, Honolulu, Hawaii, AIAA2008-6919, 18-21 August, 2008.

[11] Ueno M, Kohzai T and Koga S. Transonic Wind Tunnel Test of the NASA CRM (Volume1). *JAXA Research and Development Memorandum*, JAXA-RM-13-017E, 2014.

[12] Schairer ET, Mehta RD and Olsen ME. Effects of pressure-sensitive paint on experimentally measured wing forces and pressures. *AIAA J.*, Vol.40, No.9, pp.

1830-38, 2002.

5 Contact Author Email Address

Mailto: sugioka.yousuke@aero.mech.tohoku.ac.jp

Acknowledgments

The authors wish to thank Mamoru Sato, Hiroshi Kanda, and all of the members of Supersonic Wind Tunnel Section and Transonic Wind Tunnel Section, JAXA for their kind preparation and operation of the wind tunnel test and measurement. We gratefully acknowledge helpful discussions with Shunsuke Koike, Makoto Ueno, and Tsutomu Nakajima, and all of the members of Aeronautical Technology Directorate, JAXA.

Copyright Statement

Table 1 Surface roughness of PC-PSPs

	Ra [μm]	k_{tech} [μm]
MOD-2	2.61	11.0
MOD-3	1.15	4.83

Table 2 Heights of trip disks on 3D-CRM

Fuselage [μm]	Main wings [μm]	Horizontal stabilizers [μm]
78.74	99.06 (inner) 88.90 (middle) 78.74 (outer)	78.74

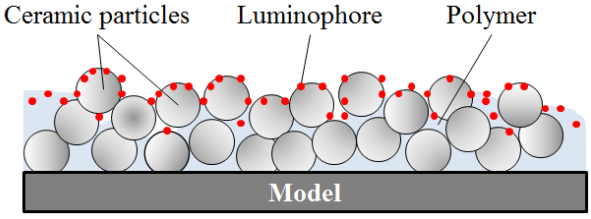

Fig. 1 Schematic of PC-PSP

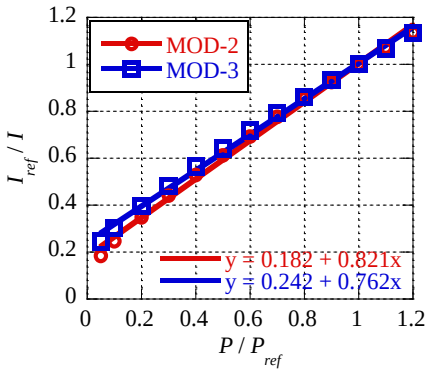

(a) Pressure Sensitivity (P_{ref} = 100 kPa, T_{ref} = 293 K)

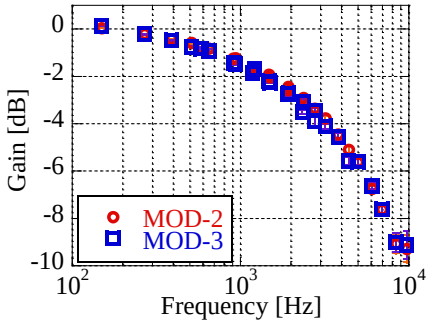

(b) Bode plot (P_{ref} = 100 kPa, T_{ref} = 293 K)

Fig. 2 Characteristics of PC-PSPs

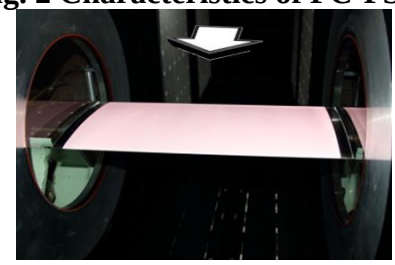

Fig. 3 2D-CRM installed in JTWT2

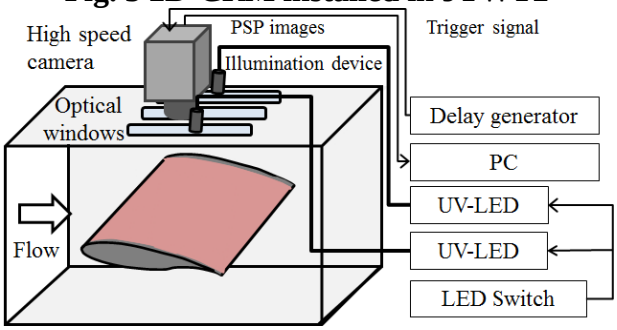

Fig. 4 PSP measurement system in JTWT2

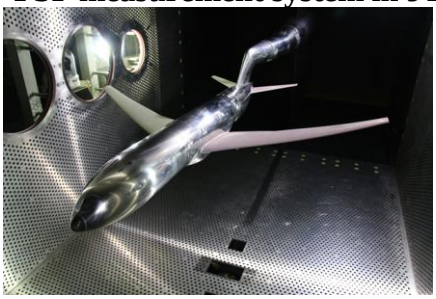

Fig. 5 3D-CRM installed in JTWT1

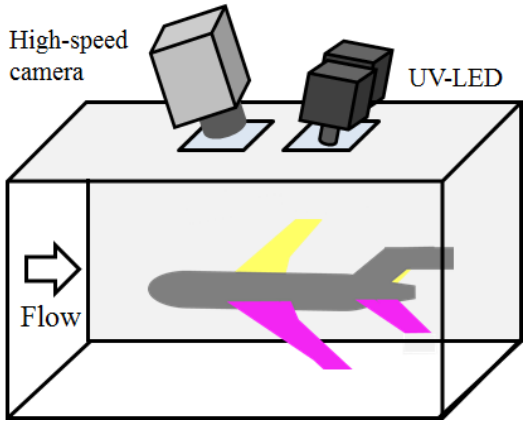

Fig. 6 PSP measurement system in JTWT1

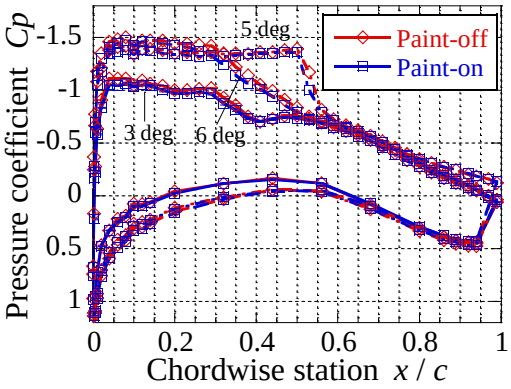

Fig. 7 Comparison of pressure distiribution on CRM airfoil between paint-off and paint-on conditions

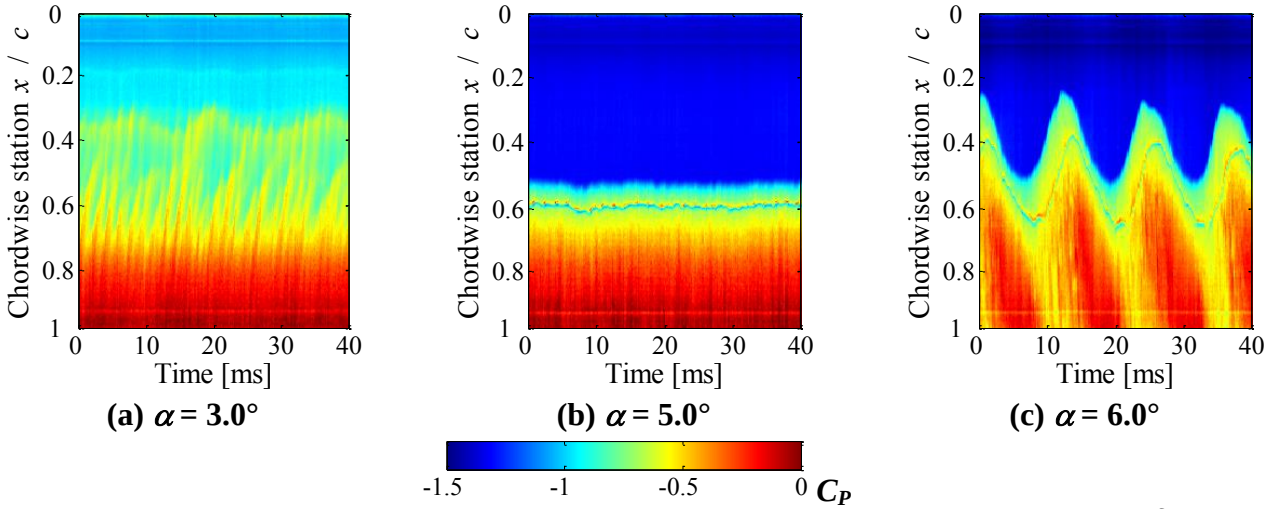

Fig. 8 Time-series pressure distiribution on 2D-CRM (M = 0.74, Re_C = 5.0 x 10^6)

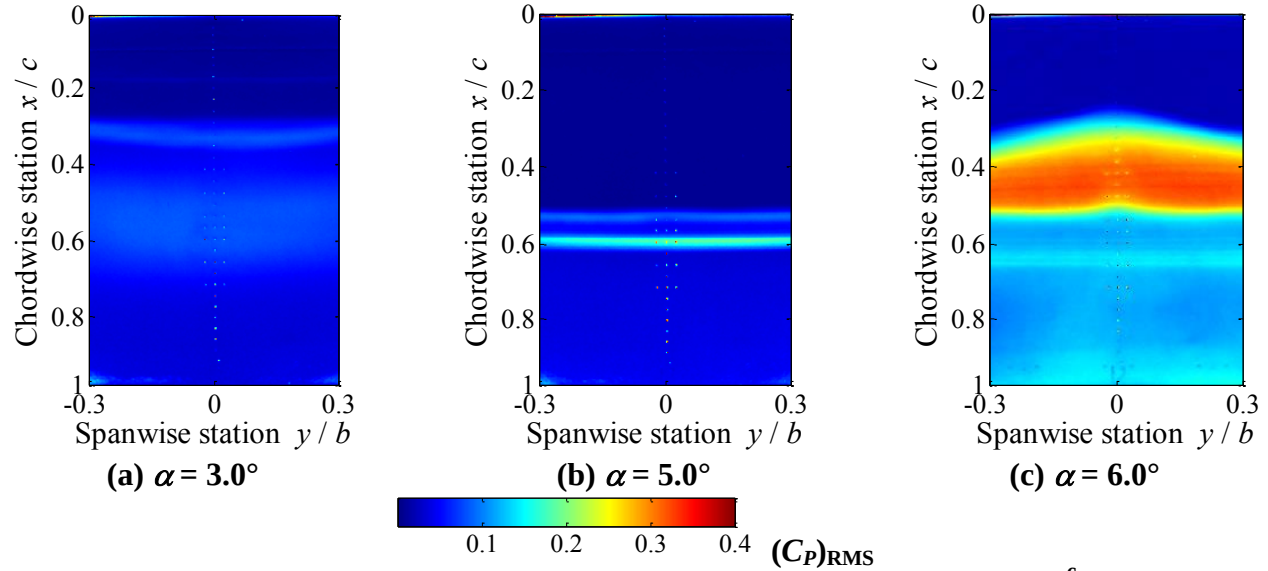

Fig.9 C_P RMS distribution on 2D-CRM (M = 0.74, Re_C = 5.0 x 10^6)

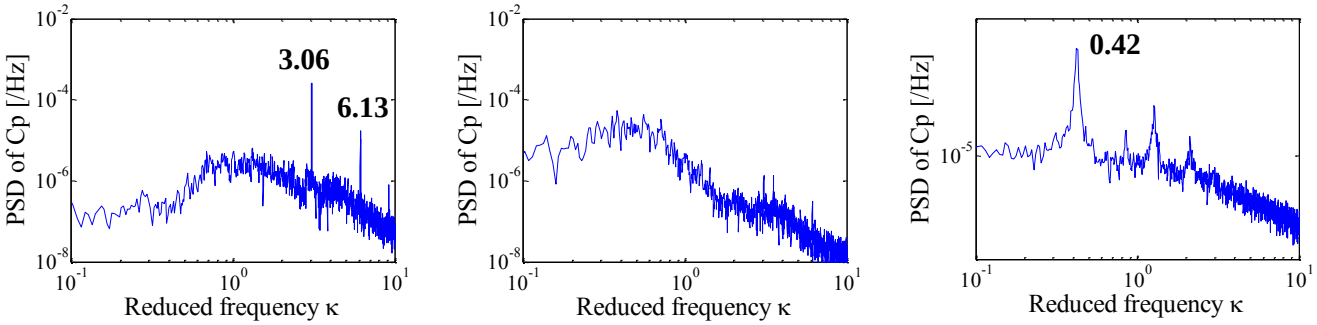

(a) α = 3.0° (x/c = 0.33) **(b) α = 5.0°(x/c = 0.53)** **(c) α = 6.0°(x/c = 0.41)**

Fig. 10 Power spectral density on 2D-CRM airfoil (M = 0.74, Re_C = 5.0 x 10^6)

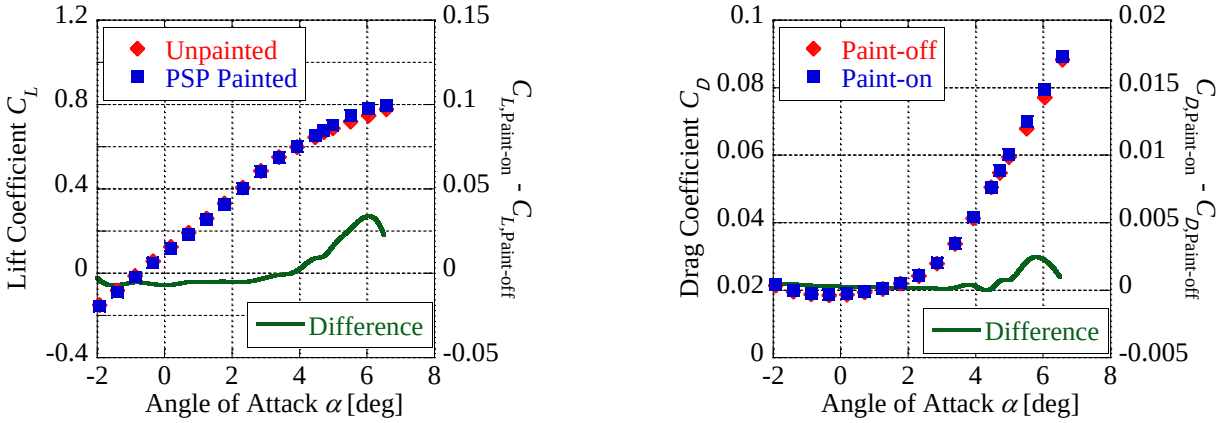

(a) Lift coefficient **(b) Drag coefficient**

Fig. 11 Comparison of Aerodynamic forces acting on 3D-CRM (M = 0.84, Re_C = 1.54 x 10^6)

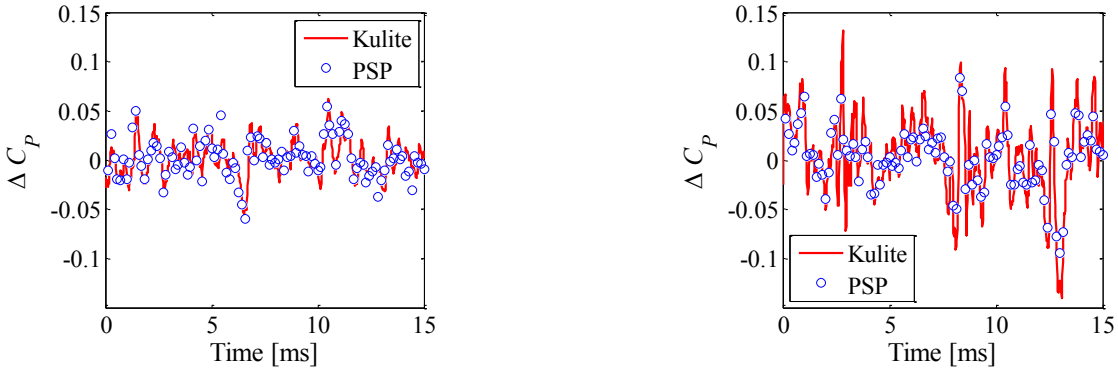

(a) α = 4.72° **(b) α = 6.58°**

Fig. 12 Comparison of pressure time histories between a Kulite sensor and PSP

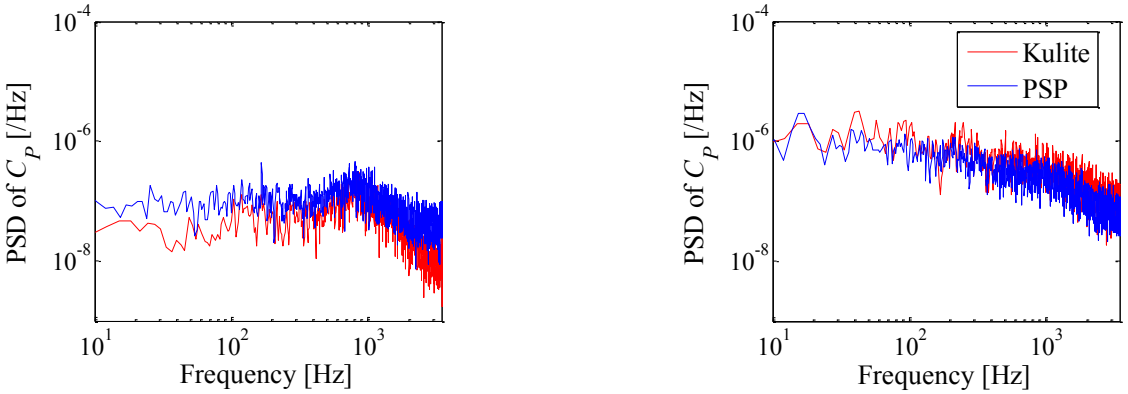

(a) α = 4.72° **(b) α = 6.58°**

Fig. 13 Comparison of PSD of ΔC_P between a Kulite sensor and PSP

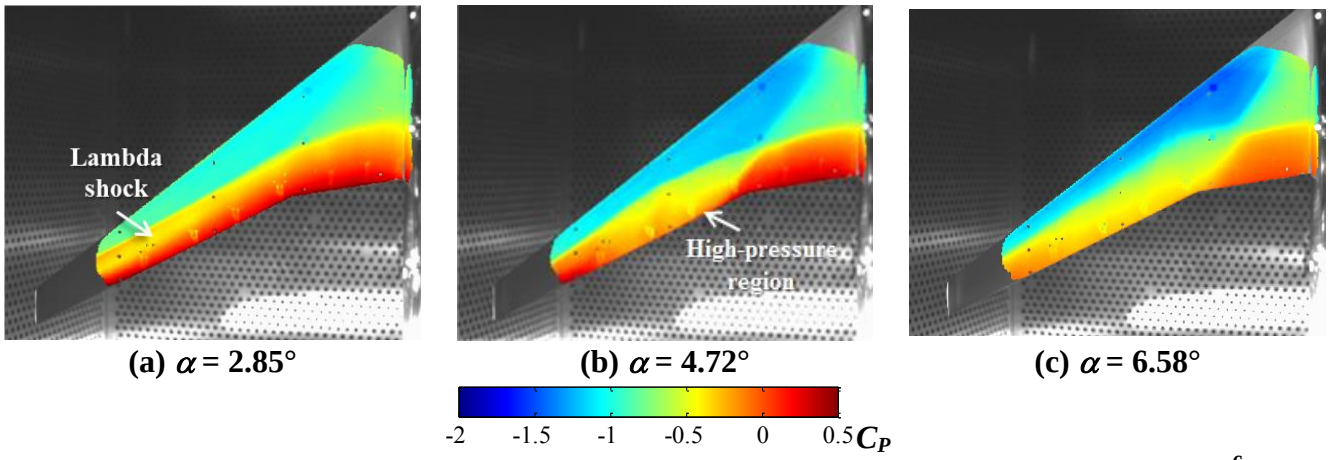

(a) $\alpha = 2.85°$ (b) $\alpha = 4.72°$ (c) $\alpha = 6.58°$

Fig. 14 Time-averaged pressure distributions on 3D-CRM (M = 0.84, Re_C = 1.54 x 10^6)

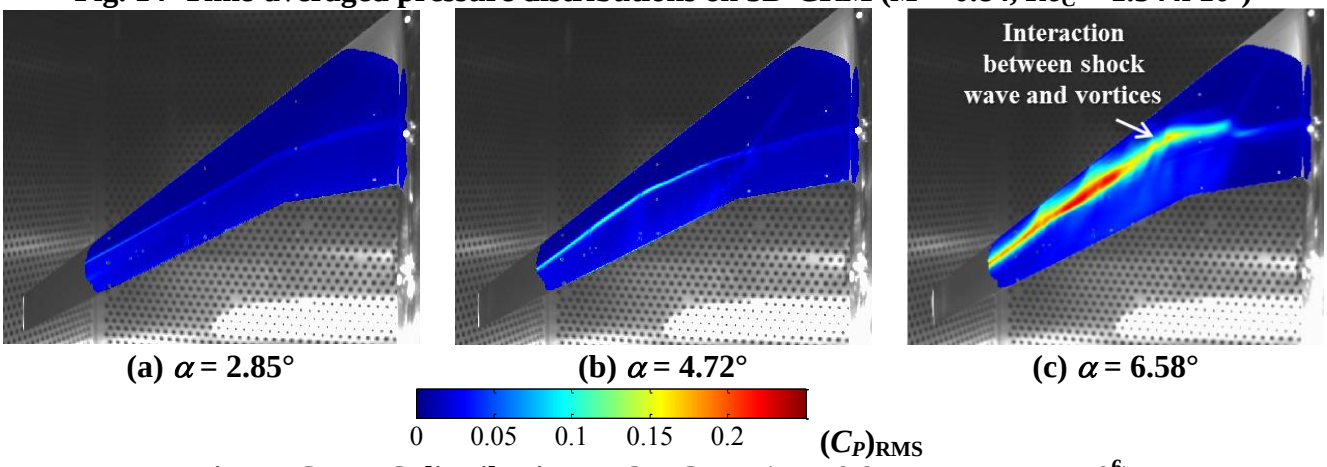

(a) $\alpha = 2.85°$ (b) $\alpha = 4.72°$ (c) $\alpha = 6.58°$

Fig.15 C_P RMS distribution on 3D-CRM (M = 0.84, Re_C = 1.54 x 10^6)

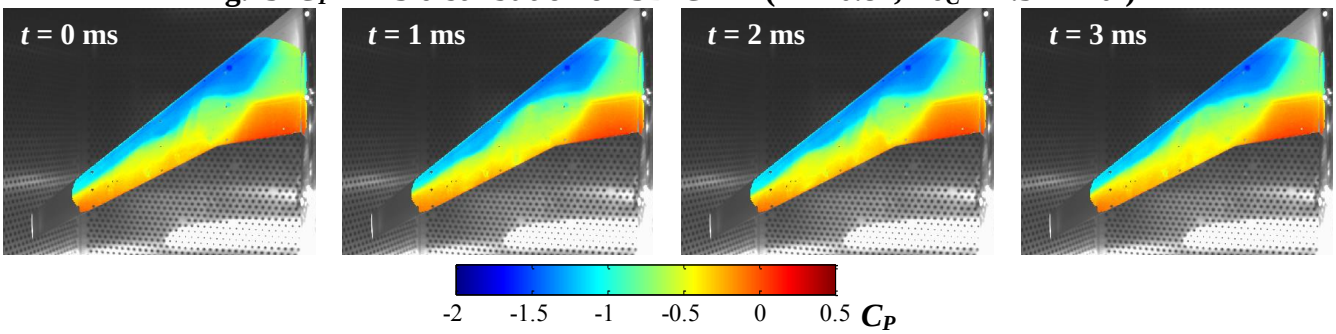

(a) Pressure coefficient time history

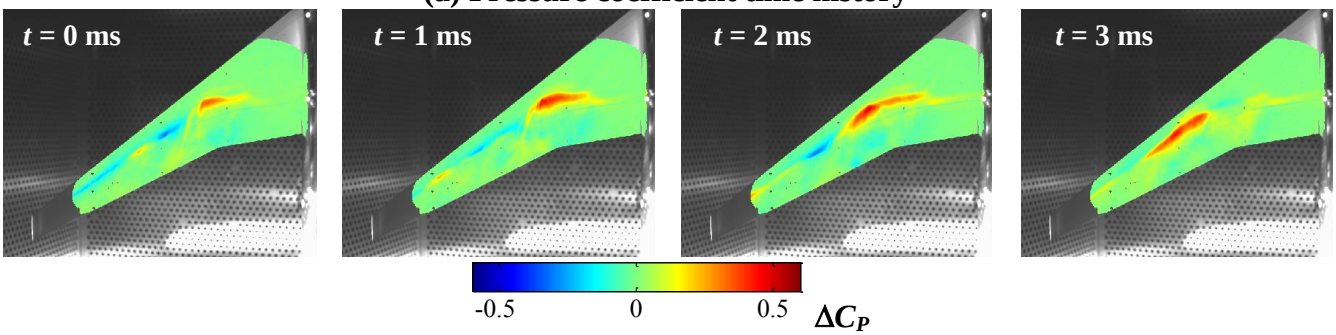

(b) AC component of pressure coefficient

Fig. 16 Time-series pressure distributions on 3D-CRM (α = 6.58°, M = 0.84, Re_C = 1.54 x 10^6)